

**Abstract.** Forthcoming CMB experiments will allow us to accurately investigate the power spectrum at very small scales ( $\ell > 1000$ ). In this context, we forecast the level of the primary anisotropies, given the actual CMB measurements. The secondary anisotropies generated after matter-radiation decoupling contribute additional power in the tail of the CMB power spectrum. Together with the primary anisotropies, we therefore compute the predicted power spectra for three dominant secondary effects induced by photon scattering. We predict these secondary contributions in flat cosmological models for parameters in agreement (to within  $2\sigma$ ) with the values allowed by current estimates.

**Key words:** Cosmology: cosmic microwave background

**A&A manuscript no.**  
(will be inserted by hand later)

**Your thesaurus codes are:**  
**missing; you have not inserted them**

# Cosmic Microwave Background anisotropies beyond the third peak

**N. Aghanim<sup>1,3</sup>, P. G. Castro<sup>2</sup>, A. Melchiorri<sup>2</sup>, and J. Silk<sup>2</sup>**

<sup>1</sup> IAS-CNRS, Université Paris Sud, Bâtiment 121, F-91405 Orsay Cedex

<sup>2</sup> Nuclear and Astrophysics Lab, University of Oxford, Keble Road, Oxford, OX 3RH, UK

<sup>3</sup> IAP-CNRS, 98 bis Boulevard Arago, F-75014 Paris

Received date / accepted date

## 1. Introduction

The last several years have been an exciting period for observational cosmology, particularly in the field of the Cosmic Microwave Background (CMB) research. With recent CMB balloon-borne and ground-based experiments such as TOCO Miller et al.(1999), , BOOMERanG de Bernardis et al.(2000), Mauskopf et al.(2000), Netterfield et al. (2001), , MAX-IMA Hanany et al.(2000), Lee et al.(2001), Stompor et al.(2001), , and DASI Halverson et al. (2001), , we are entering a new era of precision cosmology that enables us to use the CMB anisotropy measurements to constrain the cosmological parameters and the underlying theoretical models. From all of these experiments, a firm detection of the first peak in the CMB anisotropy angular power spectrum has now been obtained. Moreover, in the framework of adiabatic cold dark matter (CDM) models, the position, amplitude and width of the measured peak provide strong evidence for the inflationary predictions of a low curvature (flat) universe and a scale-invariant primordial spectrum Dodelson & Knox(2000), Melchiorri et al.(2000), . Furthermore, the latest results from BOOMERanG Netterfield et al. (2001), and DASI Halverson et al. (2001), hint at the presence of second and third peaks, confirming the theoretical prediction of acoustic oscillations in the primeval plasma and shedding new light on various cosmological and inflationary parameters de Bernardis et al. (2002), Pryke et al.(2001), Wang et al.(2001), . The next generation of CMB experiments will be even more powerful as they are designed to achieve, down to arcminute scales, accurate measurements of both the temperature anisotropies and polarised emission of the CMB. Through these data, we expect multiple oscillations in the spectrum to be unambiguously detected and, thanks

to the polarisation measurements, enable us to remove some of the degeneracies that are still affecting parameter estimation.

However, the present CMB data, as we will see in one of the following sections, already constrains the angular power spectrum of primary anisotropies with an accuracy of about  $\sim 20\%$ . The present poor determination of some of the cosmological and astrophysical parameters is more related to intrinsic degeneracies (different models leading to the same spectrum) rather than to the precision of the actual CMB measurements. On this basis, we can forecast with good accuracy the level of *primary* anisotropies on arcminute and sub-arcminute scales, where the effect of *secondary* anisotropies (i.e. produced well after matter-radiation decoupling) should start to dominate and hence significantly affect the CMB measurements. The secondary anisotropies can be generated due to photon interactions with the matter potential wells (for example in the Rees-Sciama effect Rees & Sciama(1986), , lensing Seljak(1996), and the “butterfly” effect Birkinshaw & Gull(1983), . The other secondary anisotropies are induced by the interaction of CMB photons with free electrons such as in the Sunyaev-Zel’dovich (SZ) effect Sunyaev & Zel’dovich(1980), , the Ostriker-Vishniac (OV) effect Ostriker & Vishniac(1986), Vishniac(1987), , and because of early inhomogeneous reionisation Aghanim et al.(1996), Gruzinov & Hu(1998), Knox et al.(1998), .

In the present work, we first forecast the level of primary anisotropies on sub-arcminutes scales by comparing the recent CMB data with a template of cosmological models (Section 2). We then quantify, in Section 3, the contribution of the secondary scattering effects that are likely the dominant contributions at small scales. The contributions are computed for a set of cosmological parameters allowed by the present data (within  $2\sigma$  error bars). The corresponding power spectra are presented together with our results in Section 4. Our discussion and conclusions are given in Section 5.

## 2. Forecasting primary anisotropies

Our goal in this section is to forecast the level of primary anisotropies on very small scales ( $\ell > 1000$ ), given the actual CMB measurements that span an interval in angular scales of  $2 < \ell < 1000$ . The first step in our procedure consists of building a template of cosmological models and in comparing each model with the CMB observations through a likelihood. The theoretical models of our template are computed using the publicly available CMB-FAST program. They are defined by 6 parameters sampled as follows:  $\omega_{cdm} = \Omega_{cdm}h^2 = 0.01, \dots, 0.40$  (step 0.01);  $\omega_b = \Omega_b h^2 = 0.001, \dots, 0.040$  (step 0.001);  $\Omega_\Lambda = 0.0, \dots, 1.0$  (step 0.05) and  $\Omega_k$  such that  $\Omega_m = 0.1, \dots, 1.0$  (step 0.05). The value of the Hubble constant is not an independent parameter, since  $h = \sqrt{(\omega_{cdm} + \omega_b)/(1 - \Omega_k - \Omega_\Lambda)}$ . We vary the spectral index of the primordial density perturbations within the range  $n_s = 0.60, \dots, 1.40$

(step 0.02) and we rescale the amplitude of fluctuations by a pre-factor  $C_{10}$ , in units of  $C_{10}^{COBE}$ , with  $0.50 < C_{10} < 1.40$ .

The models of the template are then compared with the recent BOOMERanG-98, DASI and MAXIMA-1 results. The power spectra from these experiments were estimated in 19, 9 and 13 bins respectively, spanning the range  $25 \leq \ell \leq 1150$ . For the DASI and MAXIMA-I experiments we use the publicly available correlation matrices and window functions. For the BOOMERanG experiment we assign a flat space for the spectrum in each bin  $\ell(\ell+1)C_\ell/2\pi = C_B$ , we approximate the signal  $C_B$  inside the bin to a Gaussian variable and we consider  $\sim 10\%$  correlations between the various bins. We consider 10%, 4% and 5% Gaussian distributed calibration errors for the BOOMERanG-98, DASI and MAXIMA-1 experiments respectively and we included the beam uncertainties by the analytical marginalisation method presented in Bridle et al.(2001). We also include the COBE data using Lloyd Knox's RADPack packages. The likelihood for a given cosmological model is then defined by  $-2\ln\mathcal{L} = (C_B^{th} - C_B^{ex})M_{BB'}(C_B^{th} - C_B^{ex})$  where  $M_{BB'}$  is the Gaussian curvature of the likelihood matrix at the peak. We then plot in the  $\ell(\ell+1)C_\ell - \ell$  plane the convolution of all the models that are consistent at 95% c.l. with the CMB data (Fig. 1). This provides us with the predicted power spectrum of the primary anisotropies as deduced from the actual data. We consequently define above this band the region where, at 95% c.l., a contribution from primary anisotropies is *unlikely* to be present. In performing the convolution of all the models, we have neglected the correlations between different  $\ell$  modes for a single model: this simple procedure is also the most conservative approach. Moreover, our computations rely on two main assumptions:

- The primary CMB can be described by one of the theoretical models in our template (i.e. we do not consider possible deviations such as scale-dependent spectral indexes, isocurvature primordial perturbations or topological defects).
- The present CMB data is not affected by unknown foregrounds or systematics.

The first assumption is a theoretical prior mainly supported by the good agreement between the theoretical template and the present CMB data. The same underlying model seems also to fit the shape of the matter power spectrum on small scales obtained, for example, from recent galaxy surveys. The second assumption is based on the numerous tests performed by the experimental teams to estimate the Galactic contamination in the so-called CMB channels (150 or 30 GHz). It also relies, in particular, on the point source extraction carried out by the DASI team. Moreover, the overall consistency of the CMB data from these experiments that have sampled various regions of the sky, at different frequencies and with different techniques (bolometres and radiometres) reinforces our confidence in this second assumption. In the following, we will generalise the *standard* concept of foregrounds to include the secondary anisotropies that cannot be

spectrally disentangled from the primary anisotropies by the present experiments, and thus corrected for, and we will investigate their possible contributions.

### 3. Secondary contributions

We study the dominant contributions due to secondary effects generated through interactions with electrons. The induced temperature anisotropies contribute to the total signal at different angular scales. Between a few arcminutes to a few tens of arcminutes, the SZ effect dominates, whereas at smaller angular scales typically down to arcminute scales the extra power essentially comes from the OV effect.

#### 3.1. Sunyaev-Zel'dovich effect

The SZ effect (see Birkinshaw(1999) for a recent review) is a well-studied effect which designates the inverse Compton interaction of the CMB photons with the free electrons of the hot intra-cluster medium. This effect is usually “decomposed” into two parts: the so-called thermal SZ (TSZ) and the kinetic SZ (KSZ) effects. The TSZ amplitude is a measure of the pressure integral along the line of sight. It is directly linked to the intra-cluster gas properties (temperature  $T_e$  and optical depth  $\tau$ ). It has a very peculiar spectral signature that translates into an excess of brightness at high frequencies (850  $\mu\text{m}$ ) and a decrement at low frequencies (2 mm). For hot clusters, it can be modified to include relativistic corrections (see Rephaeli(1995) for example). The KSZ effect corresponds to a first-order Doppler effect when a galaxy cluster moves with respect to the CMB rest frame with a radial peculiar velocity  $v_r$ . The KSZ anisotropies have the same spectral signature as the primary CMB anisotropies.

The SZ effect one of the most important sources of secondary anisotropies. Due to its spectral signature, the TSZ can in principle be separated from the other components (in particular from the CMB primary anisotropies) by means of accurate multi-wavelength observations in the millimetre/submillimetre range Hobson et al.(1998), Bouchet & Gispert(1999), Snoussi et al.(2001), . The only remaining contribution is therefore that associated with the KSZ anisotropies which cannot be separated from the primary fluctuations via multi-wavelength measurements. However, most of the present and future CMB experiments due to their lack of frequency coverage are unable to detect and subtract the TSZ anisotropies from the measurements. This contribution is thus likely to be present in the measured signal. Several techniques, based on analytic computations or numerical simulations, have been used in the literature to predict the SZ signal of a cluster population (as for example in Cooray(2000), da Silva et al.(2000), Refregier & Teyssier(2000), Springel et al.(2001)). Their intrinsic differences result in different predictions, especially for the power spectrum, however they basically agree. It

is therefore important to realise that these predicted power spectra provide us an order of magnitude estimate of the effect rather than exact and precise predictions. In the present study, we investigate the SZ anisotropies using a semi-analytical model, the most recent version of which (assumptions and procedures) is described in detail in Aghanim et al.(2001), . It is based on the computation of predicted cluster numbers from a Press-Schechter Press & Schechter(1974) mass function modified according to Sheth & Tormen(1999) and Wu(2000). Each cluster is physically described by its intra-cluster gas temperature and electron density distribution. Provided with these quantities and the cluster peculiar velocity, both TSZ and KSZ anisotropies are computed for the cluster population. The SZ contribution (power spectrum) is then computed via simulated maps of both KSZ and TSZ components.

### 3.2. Inhomogeneous reionisation

It has become of common knowledge that the universe underwent reionisation that was completed around a redshift  $z_i \sim 6$ . The evidence for reionisation relies on observations of the Gunn-Peterson Gunn & Peterson(1965), effect (both in hydrogen and helium) towards distant quasars Becker et al.(2001), . Several physical processes have been proposed to achieve the total reionisation of the universe. Among them, photoionisation by early luminous sources (stars, quasars, dwarf galaxies) has recently been the most favoured. Indeed, it is a rather simple and natural scenario in which the first luminous sources emit ionising photons that ionise hydrogen atoms in their vicinities. In this model, reionisation starts as an inhomogeneous process, and the total reionisation is reached when the ionised bubbles overlap (due to their increasing number and to their expansion). The most recent observations of very distant quasars ( $z \sim 6$ ) are now suggesting that we have reached the point where we start to observe the period of inhomogeneous reionisation (IHR) Becker et al.(2001), Gnedin(2001), . As pointed out by Aghanim et al.(1996), inhomogeneous reionisation can induce secondary anisotropies of the KSZ type, when the ionised bubbles move with respect to the CMB rest frame.

As for the SZ effect, we estimate the possible contribution (in terms of power spectrum) of the anisotropies due to IHR. To do so, we will use the simple model proposed by Gruzinov & Hu(1998), which we have generalised to a non-critical universe (open or flat with non-zero cosmological constant). It is an empirical model of the IHR based on three parameters: the redshift at which ionisation starts  $z_s$ , its duration  $\delta z$  and the typical size of the ionised bubble  $R$ . In our case, we add the constraint that reionisation is completed at  $z_i = 6$ , i.e. for a given  $z_s$  this fixes  $\delta z$ . In addition, we set  $z_s = 10$  which is a reasonable assumption for the formation of the first objects, i.e. when ionisation starts. However, this simple model is limited by the fact that it gives a predicted power

spectrum for a specified bubble size that for illustration we set to 10 Mpc. A smaller (larger) size, shifts the power spectrum to smaller (larger) angular scales and decreases (increases) the amplitude.

### 3.3. Ostriker-Vishniac effect

Alongside with the IHR effect produced during the first stages of reionisation and independently of any physical model to explain the sources of photoionisation, we have to take into account the well-studied Ostriker-Vishniac effect OV Ostriker & Vishniac(1986), Vishniac(1987), Hu et al.(1994), Dodelson & Jubas(1995), Jaffe & Kamionkowski(1998), which arises during the linear regime of the cosmological density fluctuations evolution. Contrary to the IHR, this second order effect assumes a homogeneous ionisation fraction and relies entirely on the modulation of the Doppler effect by spatial variations of the density field which affect the probability of scattering. Due to its density squared weighting, it peaks at small angular scales, typically arcminute scales in low matter-density flat models, and produces  $\mu K$  rms temperature anisotropies.

To estimate its power spectrum, and therefore its contribution to the temperature anisotropies, we follow the Jaffe & Kamionkowski(1998) approach. The OV effect can be expressed as the time integral of the velocity field projection along the line of sight modulated by the density field and weighted by the so-called visibility function. The visibility function gives the probability of rescattering of the photons as a function of time (or  $z$ ) and encodes all the information relevant for reionisation. The usual approach is to consider that the visibility function follows a Gaussian centred near  $z_i$  with a width corresponding to the interval of reionisation  $\delta z$ . This describes an idealised model for the evolution of the reionisation process. However, cosmological simulations Gnedin(2000), Gnedin(2001), , supported by recent observational data from SLOAN Becker et al.(2001), , indicate a slow first stage of reionisation, called the pre-overlap phase, followed by a fast overlap and post-overlap periods around  $z_i \simeq 6$ . We thus propose a more realistic model for the visibility function which shape consists of a curve with a smooth growing slope at redshifts higher than  $z_i$  and a steep decrease just before  $z_i$ . This approach increases the amplitude of the OV power spectrum by 50% at all scales and produces a slight shift of its peak to smaller multipoles (larger angular scales) as compared to previous works. This simple but efficient analytical modeling of the OV effect will depend on the reionisation redshift, its duration and the cosmological model.

## 4. Results

The main results of our work are plotted in Figure 1. Constraints on the primary anisotropies are plotted assuming the template of models described in Section 2. As we

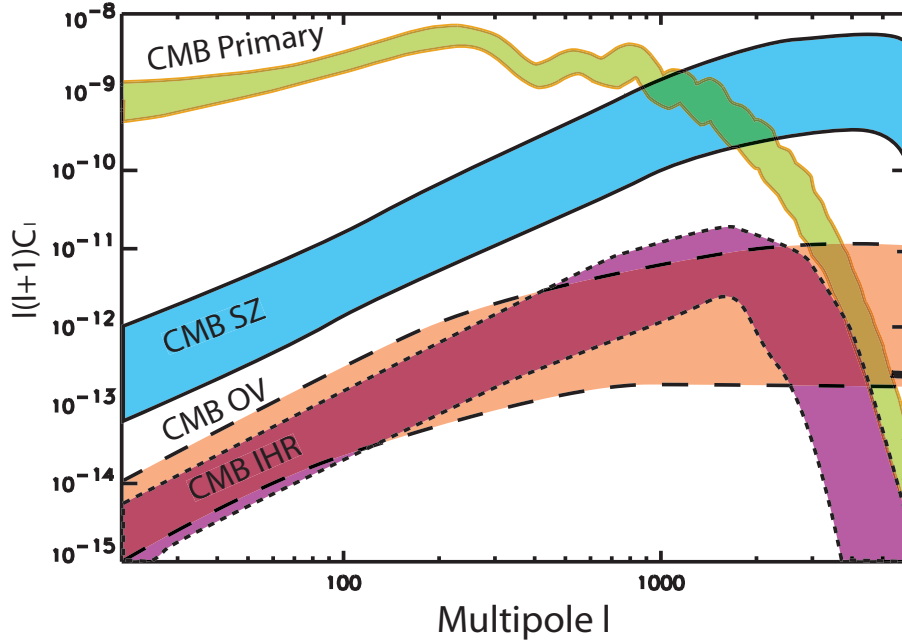


**Fig. 1.** Primary and Secondary CMB anisotropies. The 95% confidence levels for the primary anisotropies (see text) are plotted together with the extreme predictions allowed (within  $2\sigma$ ) by the present parameter estimations. The SZ (TSZ+KSZ) effect at 150 GHz is displayed in solid lines, the IHR and OV contributions are plotted with dotted and dashed lines, respectively.

can see, even if multiple oscillations in the CMB data have not been detected at a level better than  $2\sigma$  (see, e.g. Douspis & Ferreira(2001)) the actual data can constrain the region of compatible theoretical models. In particular, the level of primary anisotropies for  $\ell > 1000$  can be well defined, suggesting that measurements of the power around the first 3 peaks constrain the intrinsic parameters of the model template. Together with the primary anisotropies, we have computed predicted power spectra for secondary anisotropies in the case of 6 extreme flat cosmological models with parameters  $\omega_{cdm} = 0.06 - 0.18$  and  $h = 0.55 - 0.87$  and  $\omega_b = 0.018 - 0.022$ , in agreement (within  $2\sigma$ ) with the values allowed by the CMB analysis Melchiorri & Silk(2002), and the HST measurements of the Hubble parameter Freedman et al.(2001), . In figure 1, we display the extreme predicted spectra constituting the envelope of the possible contributions.

As far as the SZ effect is concerned, we emphasize that the majority of present experiments cannot disentangle it from the primary CMB due to their observing frequencies. We therefore calculate the TSZ contribution at two frequencies representative of the present

experiments: 30 GHz for the radiometric (DASI and CBI-like) experiments and 150 GHz for the bolometric (BOOMERanG, MAXIMA and ARCHEOPS-like) experiments. This component is then added to the KSZ contribution; the total SZ power is then plotted. The SZ power spectrum peaks between  $\ell \sim 3200$  and  $3600$  depending on the cosmological model (but independently of the frequency). Its maximum power, in turn, depends more strongly on the set of cosmological parameters and obviously on the frequency. At 30 GHz, the  $\ell(\ell+1)C_\ell$  range between  $\sim 2 \cdot 10^{-8}$  and  $\sim 2 \cdot 10^{-9}$ . At 150 GHz, the maximum is in between,  $5 \cdot 10^{-10}$  and  $1 \cdot 10^{-9}$ . We emphasize again that these predictions ought not to be taken at face value, but rather as indicative amplitudes for the SZ effect. The two other secondary effects induces temperature fluctuations. They can be directly expressed in terms of their power spectra regardless of the frequency. The power spectrum of secondary anisotropies generated during the inhomogeneous reionisation peaks in between  $\ell \sim 1100$  and  $1800$  with an amplitude comprised between  $\sim 10^{-11}$  and  $3 \cdot 10^{-12}$ . As for the OV contribution, the power spectrum peaks around the multipoles  $\ell = 2000 - 4000$ , where the primary anisotropies become subdominant, and its amplitude in  $\ell(\ell+1)C_\ell$  varies roughly between  $10^{-13}$  and  $10^{-11}$ .

It is worth noting that the SZ anisotropies constitute the dominant secondary contribution when the TSZ effect is not removed, as is the case in the present study. When we compare the power of the primary and secondary anisotropies (Fig. 1), we find that the highest secondary contribution obtained for the model ( $w_b = 0.018$ ,  $w_{cdm} = 0.06$ ,  $h = 0.87$ ) equals the primary power spectrum for  $\ell \sim 1000$  at 150 GHz. At lower frequencies (e.g. 30 GHz), this equality takes place at  $\ell \sim 600$ . In this extreme but allowed (at  $2\sigma$ ) cosmological model, the secondary anisotropies are expected to significantly contribute to the signal for  $\ell > 600$  (at 150 GHz) and  $\ell > 200$  (at 30 GHz). As displayed in figure 2, the observed (total) power spectrum would have been severely modified already at the position of the second acoustic peak.

## 5. Discussion and Conclusions

In this study, we have examined the sub-arcminute structure of the angular power spectrum of the CMB anisotropies. Using a Bayesian approach, we have shown that under the assumption of a wide class of inflationary adiabatic CDM models, the present CMB data on degree and sub-degree scales can be used to forecast the level of anisotropies. We have therefore put strong bounds on the level of contribution from primary CMB anisotropies to the overall spectrum for  $\ell > 1000$  (on sub-arcminutes scales). These predictions rely on the experimental results and assume that the present CMB data are free from any unknown foreground contamination *including secondary anisotropies*.

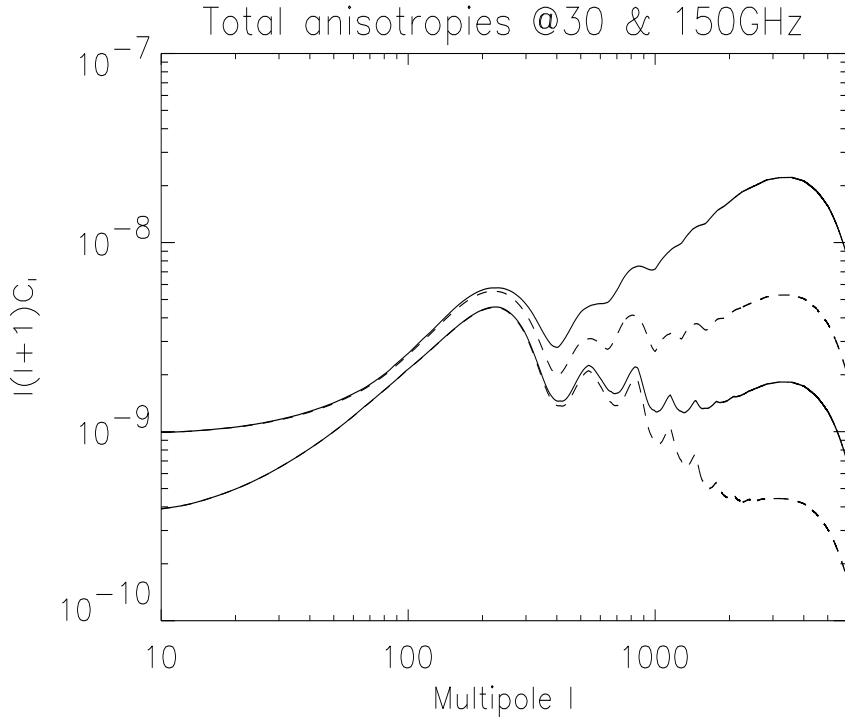


**Fig. 2.** Total CMB anisotropies. The sum of the primary and secondary anisotropies is plotted as a solid line at 30 GHz (for a DASI-like experiment) and as a dashed line at 150 GHz (for a BOOMERanG-like experiment). Only the 2 extreme cases are displayed.

We have checked that this hypothesis, and the underlying results, remain valid when we generalise the foreground to include the secondary anisotropies. We have therefore computed theoretical predictions for three dominant “candidates” for the secondary anisotropies: SZ effect, OV effect and IHR. The present status of the experiments (frequency coverage) does not allow us to remove a possible contribution from the TSZ effect of a cluster population. In this context, the secondary contribution to the CMB power spectrum is quite dominated by TSZ. However, multi-frequency observations in the millimetre and sub-millimetre would enable the removal of most of the TSZ contribution. In this case, the remaining SZ signal is associated with the KSZ effect. It is one order of magnitude lower than the values quoted in figure 1, and has the same spectral signature as the primary anisotropies. The remaining SZ contribution would therefore be larger than, or of the same order of, the OV and IHR contributions (which are at the same level). Since all three signals are spectrally confused, we would measure the sum of the three contributions. In addition, the correlation between the TSZ signal and the sum could help in constraining OV and IHR amplitudes. In the extreme cosmological model given by parameters allowed by the actual constraints, we have shown that the secondary

signal can be high enough to match the power of the CMB primary anisotropies after the second or third peak (at 30 and 150 GHz respectively). If this extreme contribution were possible at that level, this would strongly affect the CMB power spectrum at  $\ell > 700$  (for 150 GHz) and  $\ell > 200$  (for 30 GHz). However, this would be the case only for the extreme case ( $w_b = 0.018$ ,  $w_{cdm} = 0.06$ ,  $h = 0.87$ ). Moreover, such an effect would be present in both BOOMERanG and DASI data (at 150 and 30 GHz respectively) with different amplitudes while the data are consistent. Consequently, either the corresponding cosmological model is ruled out, or we can conclude that *the present CMB data can already constrain the contribution from the secondary effects, TSZ effect in particular*. This contribution is indeed highly dependent on the cluster abundance and their internal physics which can modify our predictions. In addition, this result has been obtained under a theoretical prior. The possible presence of “non-standard” mechanisms like primordial voids Sakai et al.(1999), , bumps Griffiths et al.(2001), , scale dependence of the primordial spectral index Kosowsky & Turner(1995), or topological defects Avelino & Martins(2000), , for example, can significantly change our conclusions. Fortunately, these mechanisms can be distinguished in principle from the models reported here by combination with different datasets such as those from deep redshift galaxy surveys, for example.

Future small-scale CMB data such as that expected from CBI Mason et al.(2002), , ARCHEOPS Amblard et al.(2001), Benoit et al.(2001), , MAP and, ultimately, Planck will definitely be helpful in scrutinising our results. The measurements of the CMB anisotropies after the third peak will not only constrain the cosmological model through parameter estimation, but will also enable us to probe, via the secondary anisotropies (e.g. SZ), the formation and evolution of structures<sup>1</sup>.

*Acknowledgements.* This work was partially supported by the European TMR CMBnet. PGC is supported by the Fundação para a Ciência e a Tecnologia. NA thanks the Nuclear and Astrophysics laboratory for its “hospitality”. The authors thank P. Ferreira for helpful discussion.

## References

- Aghanim, N., Désert, F. X., Puget, J. L. & Gispert, R. 1996, A&A, 311, 1.  
 Aghanim, N., Górski, K. M. & Puget, J. L. 2001, A&A, 374, 1.  
 Albrecht, A., Coulson, D., Ferreira, P. G. & Magueijo, J. 1996, Phys. Rev. Lett., 76, 1413.  
 Amblard, A., for the ARCHEOPS collaboration astro-ph/0112205, 2001.  
 Avelino, P. & Martins, C. 2000, Phys. Rev. Lett., 85, 1370.  
 Becker, R. H., et al. 2001, AJ, 122, 2850.

<sup>1</sup> When we were about to submit this article, a similar study came out (Cooray 2002) in which the author examined the contributions from secondaries including IWS and weak lensing for the fiducial  $\Lambda$ CDM model.

- Benoit, A., et al. astro-ph/0106152, 2001.
- Birkinshaw, M. & Gull, S. F. 1983, *Nature*, 302, 315.
- Birkinshaw, M. 1999, *Phys. Rep.*, 310, 97.
- Bouchet, F. R. & Gispert, R. 1999, *New Astronomy*, 4, 443.
- Bridle, S. L., Crittenden, R., Melchiorri, A., Hobson, M. P., Kneissl, R., & Lasenby, A. N. astro-ph/0112114, 2001.
- Cooray, A. 2000, *Phys. Rev. D*, 62, 3506.
- Cooray, A. 2002, In 2001 Coral Gables conference on comsoloy and particle physics, (eds. B. Kursunoglu & A. Perlmutter; American Institute of Physics Conference Proceedings), astro-ph/020304
- da Silva, A. C., Barbosa, D., Liddle, A. R., Thomas, P. A. 2000, *MNRAS*, 317, 37.
- de Bernardis, P., et al. 2000, *Nature*, 404, 955.
- de Bernardis, P. et al. 2002, *ApJ*, 564, 559.
- Dodelson, S. & Jubas, J. M. 1995, *ApJ*, 439, 503.
- Dodelson, S. & Knox, L. 2000, *Phys. Rev. Lett.*, 84, 3523.
- Douspis, M. & Ferreira, P. G. astro-ph/0111400, 2001.
- Freedman, W. L., et al. 2001, *ApJ*, 553, 47.
- Gnedin, N. Y. 2000, *ApJ*, 535, 530.
- Gnedin, N. Y. astro-ph/01102090, 2001.
- Griffiths, L. M., Silk, J. & Zaroubi, S. 2001, *MNRAS*, 324, 712.
- Gruzinov, A. & Hu, W. 1998, *ApJ*, 508, 435.
- Gunn, J. E. & Peterson, B. A. 1965, *ApJ*, 142, 1633.
- Halverson, W., et al. astro-ph/0104489, 2001.
- Hanany, S., et al. astro-ph/0005123, 2000.
- Hobson, M. P., Jones, A. W., Lasenby, A. N. & Bouchet, F. R. 1998, *MNRAS*, 300, 1.
- Hu, W., Scott, D. & Silk, J. 1994, *Phys. Rev. D*, 49, 648.
- Jaffe, A. H. & Kamionkowski, M. 1998, *Phys. Rev. D*, 58, 043001.
- Knox, L., Scoccimarro, R. & Dodelson, S. astro-ph/9805012, 1998.
- Kosowsky, A. & Turner, M. S. 1995, *Phys. Rev. D*, 52, 1739.
- Lee, A. T., et al. 2001, *ApJ*, 561, L1.
- Mason, B., and the CBI collaboration 2002, 199th AAS meeting.
- Mauskopf, P. D., et al. 2000, *ApJ*, 536, L59.
- Melchiorri, A., et al. 2000, *ApJ*, 536, L63.
- Melchiorri, A. & Silk, J. 2002, In preparation.
- Miller, A. D., et al. 1999, *ApJ*, 524, L1.
- Netterfield, C. B., et al., astro-ph/0104460, 2001.
- Ostriker, J. P. & Vishniac, E. T. 1986, *ApJ*, 306, L51.
- Press, W. H. & Schechter, P. 1974, *ApJ*, 187, 425.
- Pryke, C., Halverson, N. W., Leitch, E. M., Kovac, J., Carlstrom, W. L., Holzappel, W. L. & Dragovan, M. astro-ph/0104490, 2001.
- Rees, M. J. & Sciama, D. W. 1986, *Nature*, 511, 611.

- Refregier, A. & Teyssier, R. astro-ph/0012086, 2000.
- Rephaeli, Y. 1995, ARA&A, 33, 541.
- Sakai, N., Sugiyama, N. & 'ichi Yokoyama, J. 1999, ApJ, 510, 1.
- Seljak, U. 1996, ApJ, 463, 1.
- Sheth, R. K. & Tormen, G. 1999, MNRAS, 308, 119.
- Snoussi, H., Patanchon, J. F., Macias-Perez, J. F., Mohammed-Djafari, A. & Delabrouille, J. astro-ph/0109123, 2001.
- Springel, V., White, M. & Hernquist, L. 2001, ApJ, 549, 681.
- Stompor, R., et al. 2001, ApJ, 561, L7.
- Sunyaev, R. A. & Zel'dovich, Ya. B. 1980, ARA&A, 18, 537.
- Vishniac, E. T. 1987, ApJ, 322, 597.
- Wang, X., Tegmark, M. & Zaldarriaga, M. astro-ph/0105091, 2001.
- Wu, J. H. P. astro-ph/0012207, 2000.